

# Characterization and source apportionment of particle number concentration at a semi-urban tropical environment

Md Firoz Khan<sup>1</sup> · Mohd Talib Latif<sup>1,2</sup> · Norhaniza Amil<sup>2,3</sup> ·  
Liew Juneng<sup>1,2</sup> · Noorlin Mohamad<sup>2,4</sup> · Mohd Shahrul Mohd Nadzir<sup>1,2</sup> ·  
Hossain Mohammed Syedul Hoque<sup>1,2</sup>

Received: 28 November 2014 / Accepted: 13 April 2015 / Published online: 1 May 2015  
© Springer-Verlag Berlin Heidelberg 2015

**Abstract** Principal component analysis (PCA) and correlation have been used to study the variability of particle mass and particle number concentrations (PNC) in a tropical semi-urban environment. PNC and mass concentration (diameter in the range of 0.25–32.0  $\mu\text{m}$ ) have been measured from 1 February to 26 February 2013 using an in situ Grimm aerosol sampler. We found that the 24-h average total suspended particulates (TSP), particulate matter  $\leq 10 \mu\text{m}$  ( $\text{PM}_{10}$ ), particulate matter  $\leq 2.5 \mu\text{m}$  ( $\text{PM}_{2.5}$ ) and particulate matter  $\leq 1 \mu\text{m}$  ( $\text{PM}_1$ ) were  $14.37 \pm 4.43$ ,  $14.11 \pm 4.39$ ,  $12.53 \pm 4.13$  and  $10.53 \pm 3.98 \mu\text{g m}^{-3}$ , respectively. PNC in the accumulation mode ( $< 500 \text{ nm}$ ) was the most abundant (at about 99 %). Five principal components (PCs) resulted from the PCA analysis where PC1 (43.8 % variance) predominates with PNC in the fine and sub-micrometre range. PC2, PC3, PC4 and PC5 explain 16.5, 12.4, 6.0 and 5.6 % of the variance to address the coarse, coarser, accumulation and giant fraction of PNC, respectively. Our particle distribution results show good agreement with the

moderate resolution imaging spectroradiometer (MODIS) distribution.

**Keywords** PCA-MLR · Particle number · Diurnal variation · Back trajectory · Fire hotspot · Aerosol size distribution

## Introduction

Atmospheric aerosol particles affect human health deleteriously. Particle exposure via dermal contact, ingestion and inhalation lead to acute and chronic effects on human health (Hu et al. 2012; Kampa and Castanas 2008). Small particles, particularly in accumulation modes, have an even greater adverse impact on human health (Leitte et al. 2011; Meng et al. 2013). Pope et al. (2004) have reported that the long-term exposure to fine particulate matter is strongly associated with a cardiopulmonary mortality risk which includes pulmonary and systemic inflammation, accelerated atherosclerosis and altered cardiac autonomic function. Exposure to airborne particulate matter has been implicitly linked to mortality and morbidity rates through studies on the systematic oxidative stress on the vasculature system, heart, lungs, blood and brain (Pope and Dockery 2006; Wan Mahiyuddin et al. 2013). Further, aerosol particles play a key role in changing global climate through the scattering and absorption of atmospheric radiation (Harshvardhan 1993; Jacobson 2002; Morales Betancourt and Nenes 2014; Ramanathan et al. 2001). For instance, tropospheric aerosol particles can have a cooling effect via two mechanisms: Firstly, particles reflect incoming solar radiation back into space and thereby alter the radiative balance of the Earth-atmosphere system. Secondly, aerosols modify the microphysics, the radiative properties and the lifetime of clouds (Haywood and Boucher 2000).

Responsible editor: Gerhard Lammel

✉ Md Firoz Khan  
mdfiroz.khan@ukm.edu.my; mdfiroz.khan@gmail.com

- <sup>1</sup> Centre for Tropical Climate Change System (IKLIM), Institute for Climate Change, Universiti Kebangsaan Malaysia, 43600 Bangi, Selangor, Malaysia
- <sup>2</sup> School of Environmental and Natural Resource Sciences, Faculty of Science and Technology, Universiti Kebangsaan Malaysia, 43600 Bangi, Selangor, Malaysia
- <sup>3</sup> School of Industrial Technology (Environmental Division), Universiti Sains Malaysia, 11800 Penang, Malaysia
- <sup>4</sup> School of Ocean Engineering, Universiti Malaysia Terengganu, 21030 Kuala Terengganu, Terengganu, Malaysia

Due to rapid industrialization and population growth, the Southeast Asian region (including Malaysia) has become highly prone to aerosol loading as a result of emissions from both natural sources and anthropogenic activities. A study by Reid et al. (2013) highlighted a complex aerosol system in Southeast Asia and emphasized the need for further study into the impact of aerosols in this region. In Southeast Asia, biomass burning has been one of the most significant sources of fine mode aerosol loading (Feng and Christopher 2013). During June–September, smoke, which predominantly originates from central and southern Sumatra as well as southern and western Borneo, is transported north-westwards when south of the equator and north-eastwards when north of the equator, to the South China Sea (Xian et al. 2013). Due to the limited number of studies on the characterization of particle number concentration (PNC) in tropical sites, this study aims to undertake the comprehensive characterization of TSP,  $PM_{10}$ ,  $PM_{2.5}$ ,  $PM_1$  mass and PNC in terms of local meteorology, synoptic and station scale wind patterns, trajectory analysis and moderate resolution imaging spectroradiometer (MODIS) fire data. This study also aims to identify the possible source groups of PNC in this tropical area using a multivariate statistical technique.

## Methodology

### Sampling site

Universiti Kebangsaan Malaysia is located in the Bangi area in the state of Selangor on the Malaysian Peninsula ( $2^{\circ} 55' 31.91''$  N,  $101^{\circ} 46' 55.59''$  E). The sampling station was situated about 65 m above the sea level and located in a residential suburban area about 20 km south of Kuala Lumpur (Fig. 1). An aerosol sampler (Environmental Dust Monitor (EDM)-SVC 365, Germany) was placed on the rooftop of the Biology Building (five storeys high) of the Faculty of Science and Technology, Universiti Kebangsaan Malaysia. The sampling site was less than 1 km away from two busy main roads (Jalan Bangi and Jalan Reko) which are commonly used by light vehicles and about 3 km away from the Utara Selatan Highway, where both heavy-duty and light vehicles travel. The site was otherwise surrounded by dense forest. The sampling was conducted between 1 and 26 February 2013, during the north-easterly monsoon period.

### Experimental measurements

The measurements of TSP/ $PM_{10}$ / $PM_{2.5}$ / $PM_{1.0}$  concentrations and PNC distribution in the range of  $0.25\text{--}32\ \mu\text{m}$  in diameter

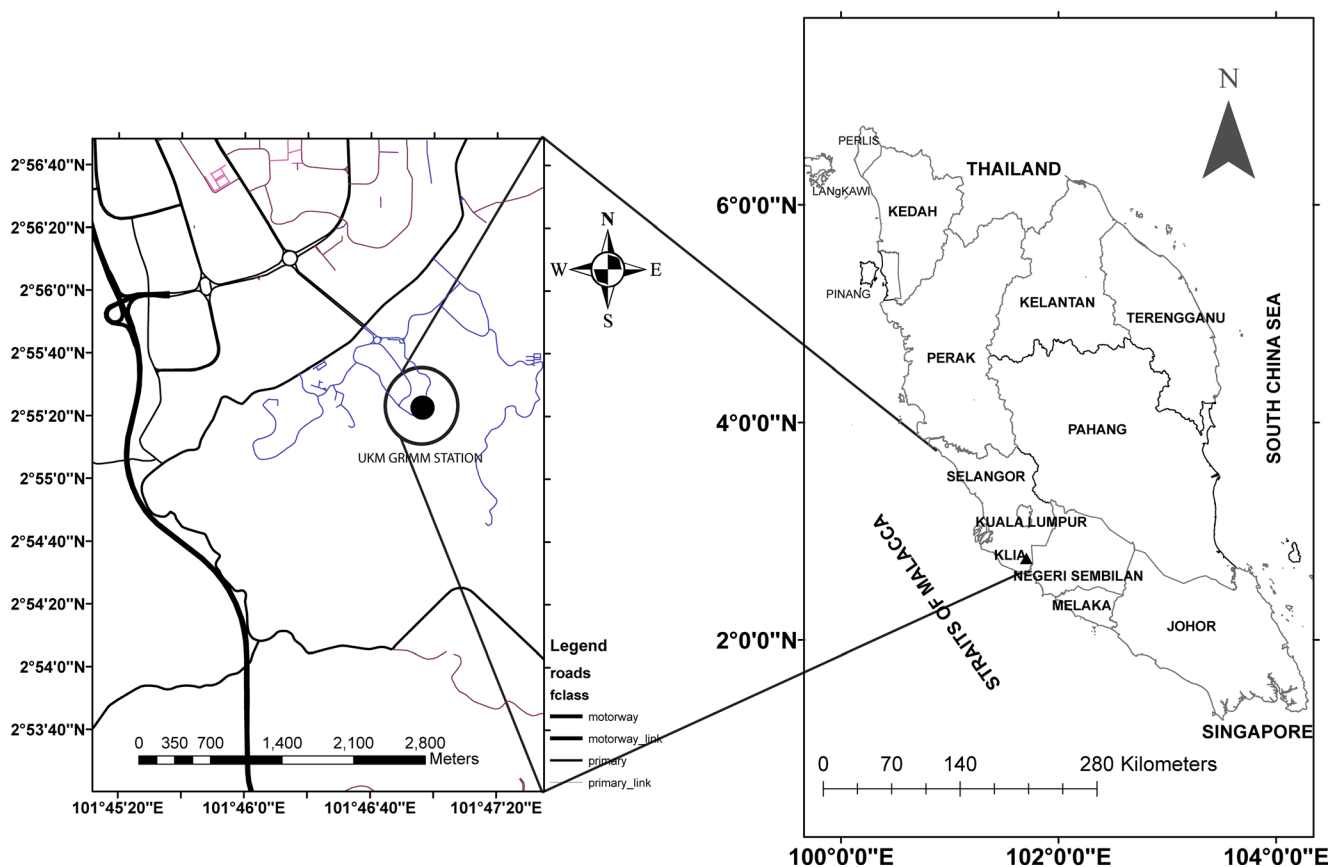


Fig. 1 Map of sampling station at UKM Bangi area

were taken simultaneously using a multi-channel Grimm aerosol spectrometer (EDM-SVC 365, Germany). The instrument can measure volatile and non-volatile components, such as sulphate, crustal material and elemental carbon, as well as semi-volatile materials, such as ammonium nitrate, some organic materials and water (Grimm and Eatough 2009; Weber et al. 2010). The aerosol spectrometer system consists of an aerosol spectrometer (Model 179) combined with two sets of sampling inlet tubes: a Nafion tube (dryer tube/non-heating tube) and a semi-volatile compound (SVC) tube (heating tube). Ambient air is directly fed into the measuring cell at a rate of  $1.2 \text{ L min}^{-1}$  using a volume-controlled pump and passes through the heart of the patented Grimm spectrometer cell that has been designed as a single particle detection and counting system. All aerosol particles passing through the measurement cell are classified by its 31 size distribution channels. It was assumed that the particles were spherical in shape, and thus, the particle mass was estimated by multiplying the obtained count concentrations with the corresponding specific density factors. These were then added to the total mass of each particulate matter channel. Following a procedure modified by Jung et al. (2010), the instrument was set for automatically controlled readings. Every 10 minutes, these alternated between the heating (at  $100 \text{ }^\circ\text{C}$ ) and non-heating tube, where the PNC was measured every minute. During the non-heating period, the temperature of the sampling tube was equal to the ambient temperature. The theoretical mass equation and measurements principle can be found in previous studies based on the light-scattering technology for single particle counts (Grimm and Eatough 2009; Technik 2006; Xiaoi et al. 2010). In the conversion process, particle diameter data was first converted into a particle volume using the mean particle diameter between the thresholds of the 31 different channels. This volume data was converted into mass distribution of particles using a density factor which Grimm had established as an ‘urban environment’ factor (Grimm and Eatough 2009). In addition to the aerosol spectrometer, the instrument was also equipped with a global positioning system (GPS) and weather station providing meteorological data, such as temperature, relative humidity and pressure level. Data was recorded at an interval of 1 min on the data storage card. The comma-separated value (CSV) data files were then analysed using the 365-SVC-Count-data-V2-5 software.

### **Contribution of synoptic wind, backward trajectory, biomass fire and the MODIS aerosol data to the particle number and mass concentration**

A synoptic wind stream is shown in Fig. 2. Every year, the south-westerly wind stream during June–September and the north-easterly wind stream during December–March blow towards the Malaysian Peninsula. These wind streams have been found to have greatly intensified PNC. To investigate

this, the synoptic wind fields at 925 hPa (500 m), latitude of  $-10^\circ$ ,  $20^\circ \text{ N}$ , longitude of  $90^\circ$ ,  $120^\circ \text{ E}$ , were plotted using the Grid Analysis and Display System (GrADS version 2.0.2). The wind field datasets were (u, v - wind) downloaded from the National Centres for Environmental Protection (NCEP)/National Centre for Atmospheric Research (<http://www.esrl.noaa.gov/psd/data/-gridded-/data.ncep.reanalysis.pressure.html>) for analysis over the sampling site. The flow pattern of the wind vector revealed a north-easterly wind in the upper right and easterly and south-easterly in the lower part of Fig. 2a, b during the first and third weeks of February 2013. The wind blew from the north-east towards the Malaysian Peninsula and then passed over the Bay of Bengal to Sumatra in Indonesia. However, the mean synoptic wind in February 2013 deviated slightly from the circulation in the third week. The mean circulation showed that the Malaysian Peninsula experienced both north-easterly and easterly wind streams.

The 3-day back trajectories were plotted online using the National Oceanic and Atmospheric Administration (NOAA)/Earth System Research Laboratory (ESRL) Physical Sciences Division website (Draxler and Rolph 2013). The mean cluster of trajectories was produced using the Hybrid Single Particle Lagrangian Integrated Trajectory Model (HYSPLIT 4.9). Figure 3a–c shows the travel path of the back trajectories, which were re-plotted using IGOR Pro 6.0.1 (WaveMetrics, OR, USA). To ensure consistency with the wind field, the releases of the trajectories were chosen at 925 hPa (500 m), and the time interval was 3 h. The fire data from MODIS represents biomass burning hotspots in the specific area of interest. Fire hotspot data was downloaded from the National Aeronautics and Space Administration-Land Atmosphere Near Real-Time Capability for Earth Observing System (EOS)-Fire Information for Resource Management System (NASA LANCE FIRMS) fire archive (<http://firms.modaps.eosdis.nasa.gov/download/>) for the range of  $8^\circ \text{ S}$  to  $20^\circ \text{ N}$  and  $90^\circ \text{ E}$  to  $120^\circ \text{ E}$  and appended onto the back trajectory graphs (Fig. 3a–c). Over the period of 1–26 February 2013, trajectories were stagnant over the Gulf of Thailand. The origin and pathway of backward trajectories in February 2013 (first and third weeks) coincided with the wind field which was plotted using GrADS software. Thus, the results of this study were validated using the output of GrADS and HYSPLIT. However, from Fig. 3c, the mean cluster of the HYSPLIT back trajectory suggests that the trajectories predominantly originated from localized sources and some of them passed over the South China Sea and inland across the Peninsula before reaching the sampling site. These results indicate that the aerosol particles in the study location of the Malaysian Peninsula originated from localized sources as well as transported over the South China Sea from regional sources, which strongly indicates the influence of long-range transport (trans-boundary) during the season studied.

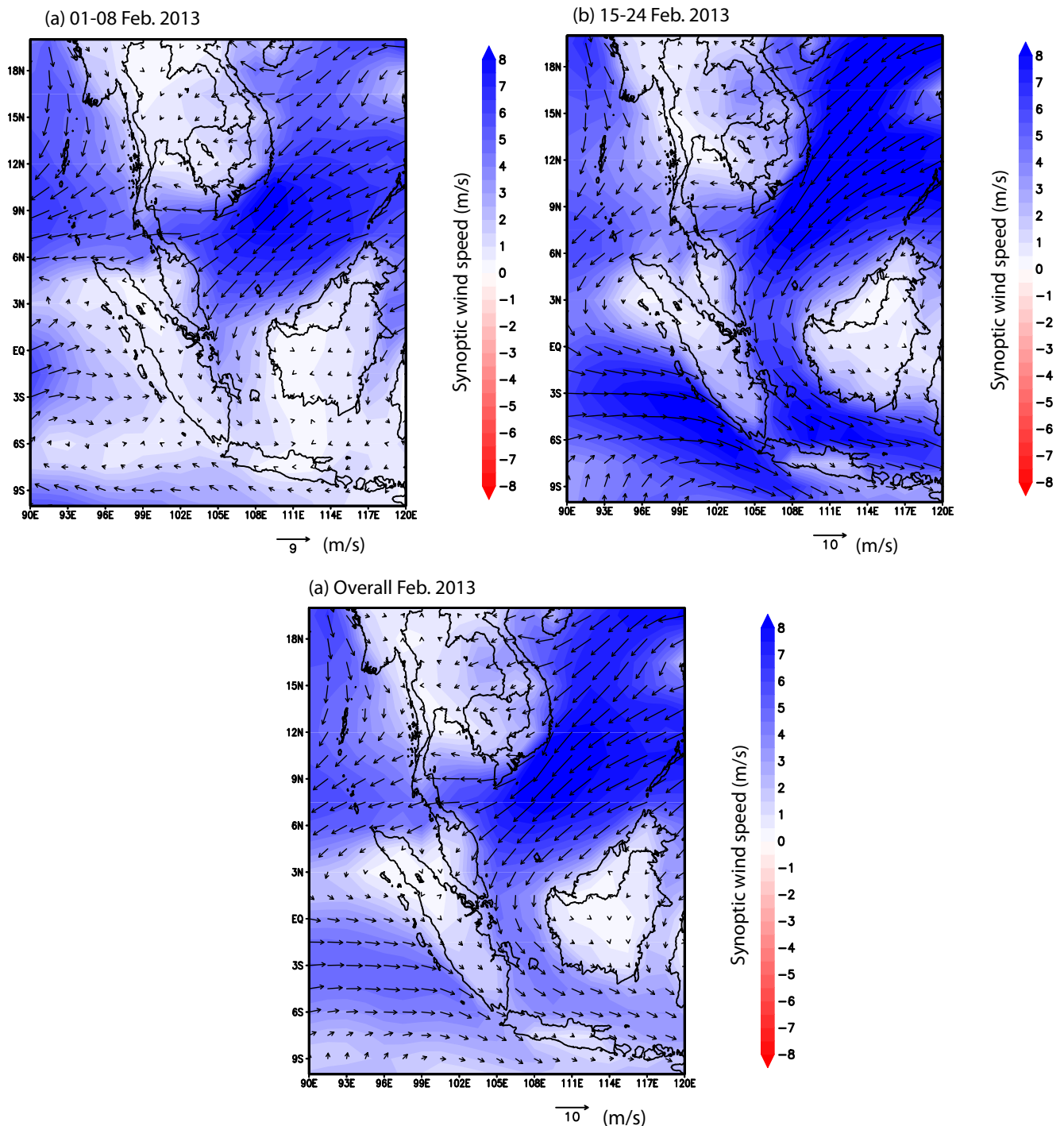


**Fig. 2** Wind vector **a** 1–8 February 2013, **b** 15–24 February 2013 and **c** overall mean of February 2013

The size distribution of aerosol data from MODIS was used to identify the sources of aerosol (Fig. 3d). The MODIS measurements were used to derive the thickness of spectral aerosol and aerosol size parameters (0.41–15  $\mu\text{m}$ ) over both land and ocean. The radius size data of aerosol particles was retrieved from NASA's Terra satellite. The red and green areas show an aerosol plume consisting of smaller (sub-micrometre

$\leq 1000$  nm) and larger particles ( $> 1000$  nm) emitted from anthropogenic sources, such as smoke from fires, industry or automobiles along with natural sources, such as windblown dust, volcanic ash and sea salts, respectively. The yellow areas show aerosol plumes where both larger and smaller particles intermingle, while the black areas indicate the lack of satellite data and recorded measurements (Fig. 3d).

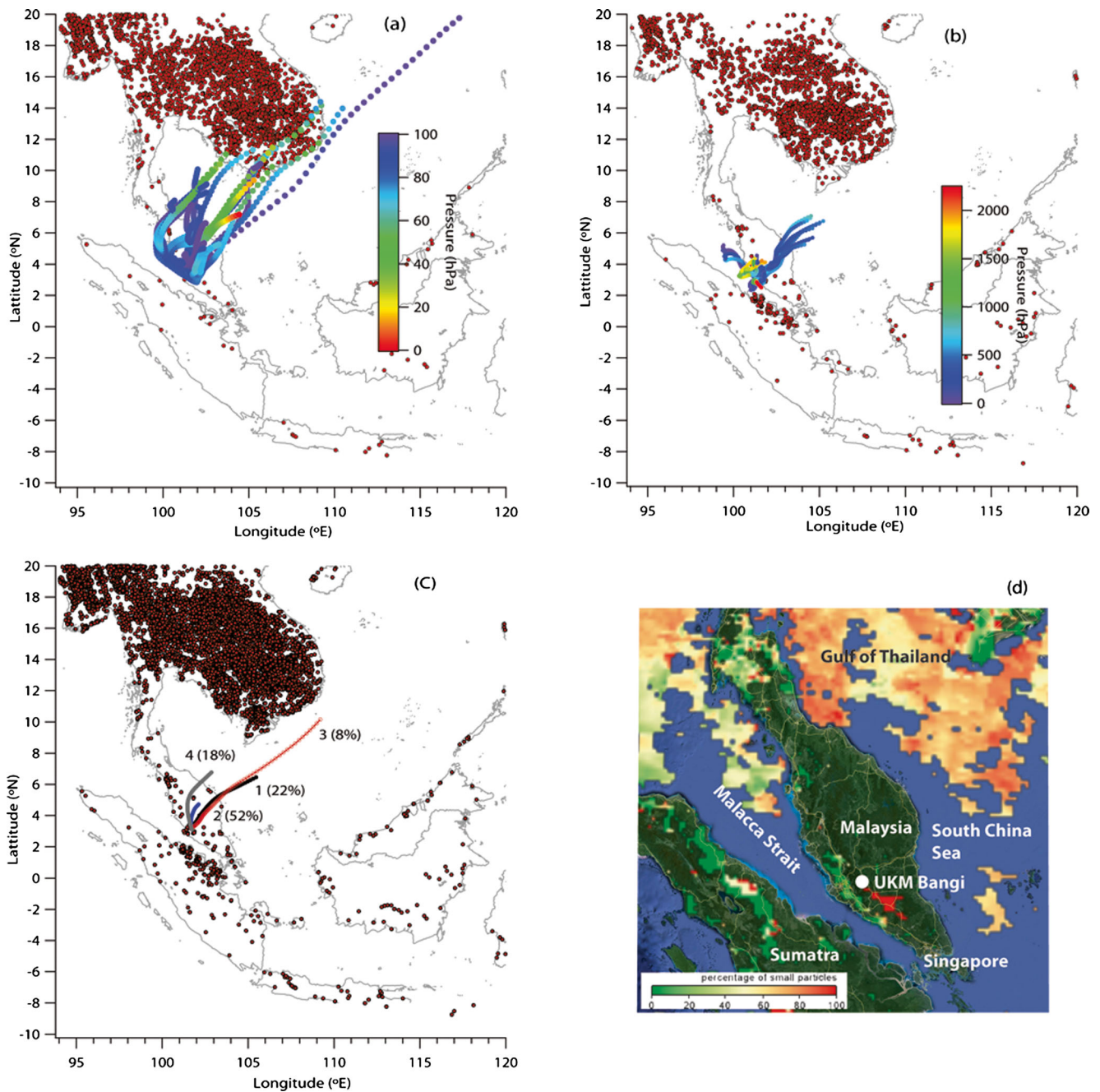


**Fig. 3** Trajectory and biomass fire hotspots **a** 1–8 Feb, **b** 15–24 Feb and **c** overall mean of Feb 2013, and **d** MODIS aerosol size distribution

**Results and discussion**

**Concentration of aerosol particle mass (TSP, PM<sub>10</sub>, PM<sub>2.5</sub> and PM<sub>1</sub>)**

The mean concentration of particles estimated from the number concentration of aerosol particles is shown in Table 1. The 24-h average mass concentrations for TSP, PM<sub>10</sub>, PM<sub>2.5</sub> and PM<sub>1</sub> were 14.37±4.43, 14.11±4.39, 12.53±4.13 and 10.53±3.98 μg m<sup>-3</sup>, respectively. The mean concentrations of the above particulate fractions are within the limits of the

Malaysian Air Quality Guideline (MAQG), the World Health Organization (WHO) and United States Environmental Protection Agency (US EPA) guidelines. Figure 4 illustrates the time series of TSP, PM<sub>10</sub>, PM<sub>2.5</sub> and PM<sub>1</sub> mass for the period. The high concentration of aerosol particles, i.e. pollution days, was observed on the 6, 8, 18 and 24 February. The 24-h mass concentrations of the particulate matter on selected pollution days are summarized in Table 2. Total daily average of PNC is 223.3 cm<sup>-3</sup>. The maximum and minimum daily average PNC are 417 and 106 cm<sup>-3</sup>, respectively. The daily results on pollution days

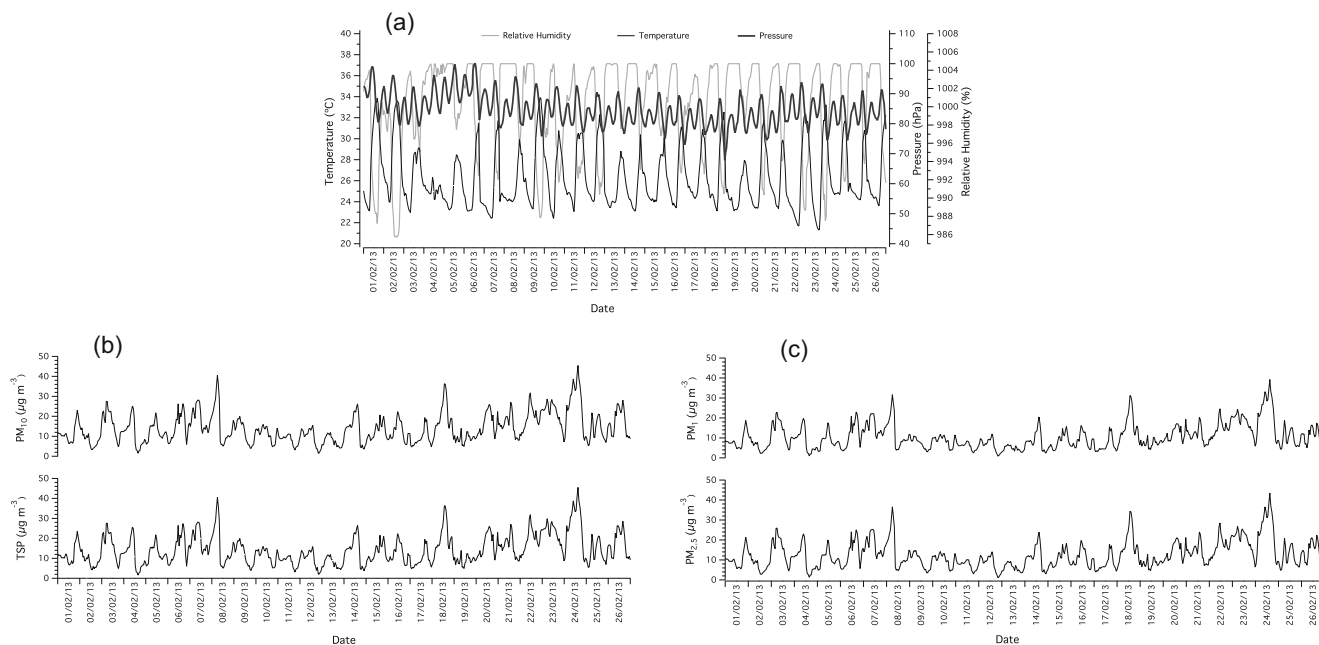
**Table 1** Summary statistics of aerosol mass ( $\mu\text{g m}^{-3}$ ) and particle number concentration (PNC) ( $\text{cm}^{-3}$ )

Variables	Mean		Median		Minimum		Maximum		Std. dev.	
	Daily	Hourly	Daily	Hourly	Daily	Hourly	Daily	Hourly	Daily	Hourly
TSP ( $\mu\text{g m}^{-3}$ )	14.37	14.30	13.05	12.50	8.65	1.60	23.53	45.55	4.43	7.43
PM <sub>10</sub> ( $\mu\text{g m}^{-3}$ )	14.11	14.04	12.78	12.37	8.44	1.45	23.04	45.47	4.39	7.44
PM <sub>2.5</sub> ( $\mu\text{g m}^{-3}$ )	12.53	12.49	10.75	11.06	7.26	1.12	20.89	43.49	4.13	6.85
PM <sub>1</sub> ( $\mu\text{g m}^{-3}$ )	10.53	10.51	9.00	8.87	5.38	0.86	18.54	39.26	3.98	6.24
PNC (total) ( $\text{cm}^{-3}$ )	223.27	223.05	175.00	189.73	106.00	16.64	417.00	821.13	94.30	141.13
PNC (<0.5 $\mu\text{m}$ ) ( $\text{cm}^{-3}$ )	216.69	216.54	170.00	182.97	102.00	15.86	409.00	788.97	93.00	137.98
PNC (>0.5 $\mu\text{m}$ ) ( $\text{cm}^{-3}$ )	6.53	6.51	6.26	5.70	4.08	0.74	10.90	32.16	1.89	4.07
PNC (1 $\mu\text{m}$ ) ( $\text{cm}^{-3}$ )	222.31	222.13	174.50	189.03	105.00	16.53	416.00	818.19	94.14	140.87
PNC (2.5 $\mu\text{m}$ ) ( $\text{cm}^{-3}$ )	0.84	0.84	0.87	0.81	0.45	0.11	1.08	2.81	0.17	0.38
PNC (10 $\mu\text{m}$ ) ( $\text{cm}^{-3}$ )	0.08	0.08	0.08	0.06	0.04	0.01	0.19	0.30	0.03	0.06

showed higher concentrations of particle mass with larger variability. On these days, the temperature range recorded was 21.2–34.7 °C and relative humidity (RH %) varied in the range 39.8–100 %. On the pollution days, high relative humidity was accompanied by low temperature. At lower temperatures, the precursor gases transform to the aerosol phase through gas-to-particle transformation reactions. In ambient conditions, the temperature in the saturated air mass is lower, such that the vapour pressure of the saturated air mass decreases. Thus, the air mass is accompanied by a substantial increase in relative humidity or achieves super saturation (>100 %), thereby contributing to the growth of aerosol particle mass or cloud droplets (Hinds 1999; Seinfeld and Pandis 2006). However, whether or not a particle initiates nucleation-

condensation depends on its size, shape, chemical composition, surface structure and surface charge (Hinds 1999).

The time series plots, as shown in Fig. 5, were examined for variations in PNC and to observe abrupt increases in concentration, condensational growth or transportation of aged particles. At the beginning of the data analysis, the number concentration of aerosol particles was sub-grouped into two categories in order to represent various modals (accumulation and coarse mode): (1)  $\leq 500$  and (2)  $> 500$  nm. Kittelson et al. (2004, 2006) distinguished aerosol particles in the size range 30–500 nm as the accumulation or soot mode. However, Řimnáčová et al. (2011) described particle sizes of  $> 100$  nm as the accumulation mode. As the cut-off points for Grimm samplers are 0.50 and 0.65  $\mu\text{m}$ , the modal limits of  $\leq 0.50$  and

**Fig. 4** Time series of TSP, PM<sub>10</sub>, PM<sub>2.5</sub>, PM<sub>1</sub>, RH (%), pressure (hPa) and temperature (°C) using 1-min interval data

**Table 2** Twenty-four-hour mass concentration particulate matters during selected pollution days

Variable	6 February	8 February	18 February	24 February
TSP ( $\mu\text{g m}^{-3}$ )	16.23±6.10	15.75±10.58	18.20±9.25	20.99±13.26
PM <sub>10</sub> ( $\mu\text{g m}^{-3}$ )	16.05±5.91	15.54±10.58	17.80±9.30	20.89±13.24
PM <sub>2.5</sub> ( $\mu\text{g m}^{-3}$ )	14.54±5.96	13.79±9.35	16.63±8.79	19.77±12.67
PM <sub>1</sub> ( $\mu\text{g m}^{-3}$ )	12.45±5.86	11.85±8.09	14.84±7.98	17.90±11.49

$\geq 0.65 \mu\text{m}$  were set for the accumulation and coarse modes, respectively. Ninety-nine per cent of the particles were assigned to the accumulation mode ( $< 500 \text{ nm}$ ), and only 1 % of the particles were assigned to the coarse mode ( $> 500 \text{ nm}$ ). The range of particle sizes, from  $0.25$  to  $> 32 \mu\text{m}$ , is also considered in the time series plots. An abrupt increase in accumulation mode particles was observed on the pollution days. The number of particles rapidly decreases once they reached an apex. Several atmospheric mechanisms, such as diffusion on surfaces, evaporation and coagulation, might play an important role in this phenomenon. When two particles collide due to Brownian motion (coagulate), they form a larger particle. Thus, coagulation reduces PNCs and shifts the distribution to a greater size (Hinds 1999; Whitby et al. 1975; Zhu et al. 2002). Air masses transported to the Malaysian Peninsula during the south-westerly wind and north-easterly wind events (Fig. 2) may well have played a significant role in increasing aged aerosol particles.

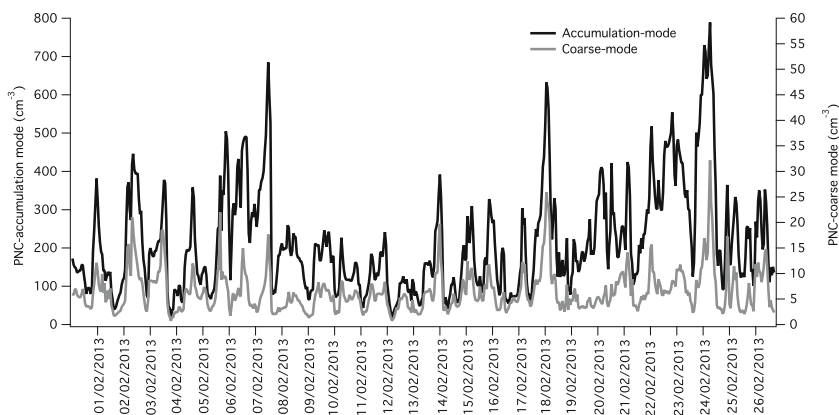
The back trajectories from the first and third week of February are also in good agreement with the synoptic wind fields. The results of the trajectory analysis indicate that the polluted air masses have originated from the biomass burning-prone region, particularly from the north-east direction and have been transported to the sampling site (Fig. 3a–b). The mean cluster of the HYSPLIT model produced trajectories arriving predominantly from localized sources as well as from the north-east direction (Fig. 3c). Furthermore, the MODIS data showed the distribution of smaller sub-micrometre ( $\leq 1000 \text{ nm}$ ) particles over the Selangor region in February 2013 (Fig. 3d). A study by Badarinath et al. (2004) observed the highest concentration of aerosol mass in the size range of

$650\text{--}1100 \text{ nm}$  occurred during a day on which biomass burning occurred compared to concentrations on days pre- and post-burning. Referring to our site in particular, good agreement was observed between the particle distribution results and the MODIS distribution indicators.

**Diurnal variations of TSP, PM<sub>10</sub>, PM<sub>2.5</sub> and PM<sub>1</sub>**

The measurements were divided into two groups. Intense hazy and cloudy days with high aerosol concentrations during the experiment are regarded as pollution days. Rest of the measurement days are regarded as non-pollution days. Several processes influence the variability of particle concentration during the daytime and night-time. The diurnal variations of PNC and precursor gases are shown in Fig. 6i, ii (a, b, and c). The 24-h variation pattern was very similar during pollution and non-pollution days (Fig. 6). However, the concentrations of particle mass, PNC and trace gases ( $\text{CO}$ ,  $\text{O}_3$  and  $\text{NO}_2$ ) were higher on pollution days (Fig. 6i (a, b, and c)) compared to non-pollution days (Fig. 6ii (a, b, and c)). During pollution days (Fig. 6i (a, b)), TSP, PM<sub>10</sub>, PM<sub>2.5</sub> and PM<sub>1</sub> concentrations decline sharply between 8:00 and 11:00. The sun’s radiation warms the surface, and air masses start rising and mixing with the surrounding air, so the boundary layer is well mixed and reaches its deepest during the day. As a result, the dispersion of pollutants is high during this time. A similar downward trend in TSP, PM<sub>10</sub>, PM<sub>2.5</sub> and PM<sub>1</sub> was observed on non-pollution days between 10:00 and 12:00 (Fig. 6ii (a and b)). On non-pollution days, the concentration remained stable after the sharp decline until the increasing point, whereas on pollution days, the concentration showed variation after the sharp

**Fig. 5** Time series of accumulation and coarse mode particles



downward phase. The change in cloud cover will alter the amount of radiation reaching the surface and the boundary layer mixing, and dispersion of pollutants will also change accordingly. The stagnant period at night favours the accumulation of aerosol particle mass and at the same time temperature inversion prevails, which eventually makes the air mass stable thereby reducing dispersion. This process generally occurs under stable atmospheric conditions (Galindo et al. 2013). However, in general, the wind speed increases substantially during the day, causing dispersion of the aerosol particle mass. At the present location, the wind speed was recorded as  $9.1 \pm 5.4 \text{ km h}^{-1}$  and  $7.1 \pm 4.5 \text{ km h}^{-1}$  for day and night, respectively. The dilution effect in the lower planetary boundary layer (PBL), along with relatively higher ambient and surface temperature as well as higher wind speed, results in lower concentrations of aerosol particles (Choi and Choi 2008). This dilution effect is generally observed during the daytime (Chow et al. 1999).

The PNC variation for all sizes showed a similar pattern (Fig. 6i (b), ii (b)). The diurnal variation of PNC can be explained by traffic frequency and the dynamics of atmospheric motion. The PNC diurnal variation is mainly caused by meteorological conditions such as solar radiation, formation of the connectively mixed boundary layer (CBL) and wind conditions (Cyrus et al. 2008). CO and NO<sub>2</sub> profiles showed similar temporal variation to that observed for PNC (Fig. 6i (c), ii (c)). Between 6.00 and 9.00, the concentration of CO and NO<sub>2</sub> is high. After 9.00, the concentration curves were flat, and the values were lower than the earlier times. The concentration of PNC and NO<sub>2</sub> depends on traffic emissions and turbulent dilution generated by traffic movement and wind (Johansson et al. 2007). Moreover, Durant et al. (2010) showed that the early morning correlation between PNC and NO<sub>2</sub> were stronger than later in the morning when mixing is greater. High O<sub>3</sub> concentrations were observed on both pollution and non-pollution days (Fig. 6i (c), ii (c)). During pollution days, with high concentrations of NO<sub>2</sub> at night or in the early morning (Fig. 6i (c)), ozone reacts with NO<sub>2</sub> to form NO<sub>3</sub> which rapidly reacts with NO<sub>2</sub> to form N<sub>2</sub>O<sub>5</sub>. The N<sub>2</sub>O<sub>5</sub> reacts with water droplets to form a larger nitrate particle. However, this pathway is not favourable in the daytime as observed by Richards (1983). Thus, the high concentration of O<sub>3</sub> and NO<sub>2</sub> at night and early morning favours the larger concentrations of PNC (Fig. 6i (b)).

### Correlations and source apportionment analysis

For a better understanding of the relationships between the variables, the Spearman correlation multivariate statistical technique and principal component analysis (PCA) were used as shown in Tables 3 and 4, respectively. The 1-h resolution of TSP, PM<sub>10</sub>, PM<sub>2.5</sub>, PM<sub>1</sub> and PNC, as measured in February 2013, were used in this analysis. The correlation analysis

**Fig. 6** Diurnal variability of TSP, PM<sub>10</sub>, PM<sub>2.5</sub>, PM<sub>1</sub>, particle number concentration (PNC (>10, ≤10, 2.5 and 1 μm)) and trace gases (CO, O<sub>3</sub>, NO<sub>2</sub> and SO<sub>2</sub>) during pollution and non-pollution days

showed that PM<sub>1</sub> and PNC (0.27–0.43 μm) are significantly correlated ( $R > 0.90$ ). Thus, the concentration of particle number and mass is dominantly within the sub-micrometre mode. A similar observation was reported by Xu et al. (2013) in which 97 % of particles were attributed to the sub-micrometre ( $N_{0.25 < d < 1 \mu\text{m}}$ ) range.

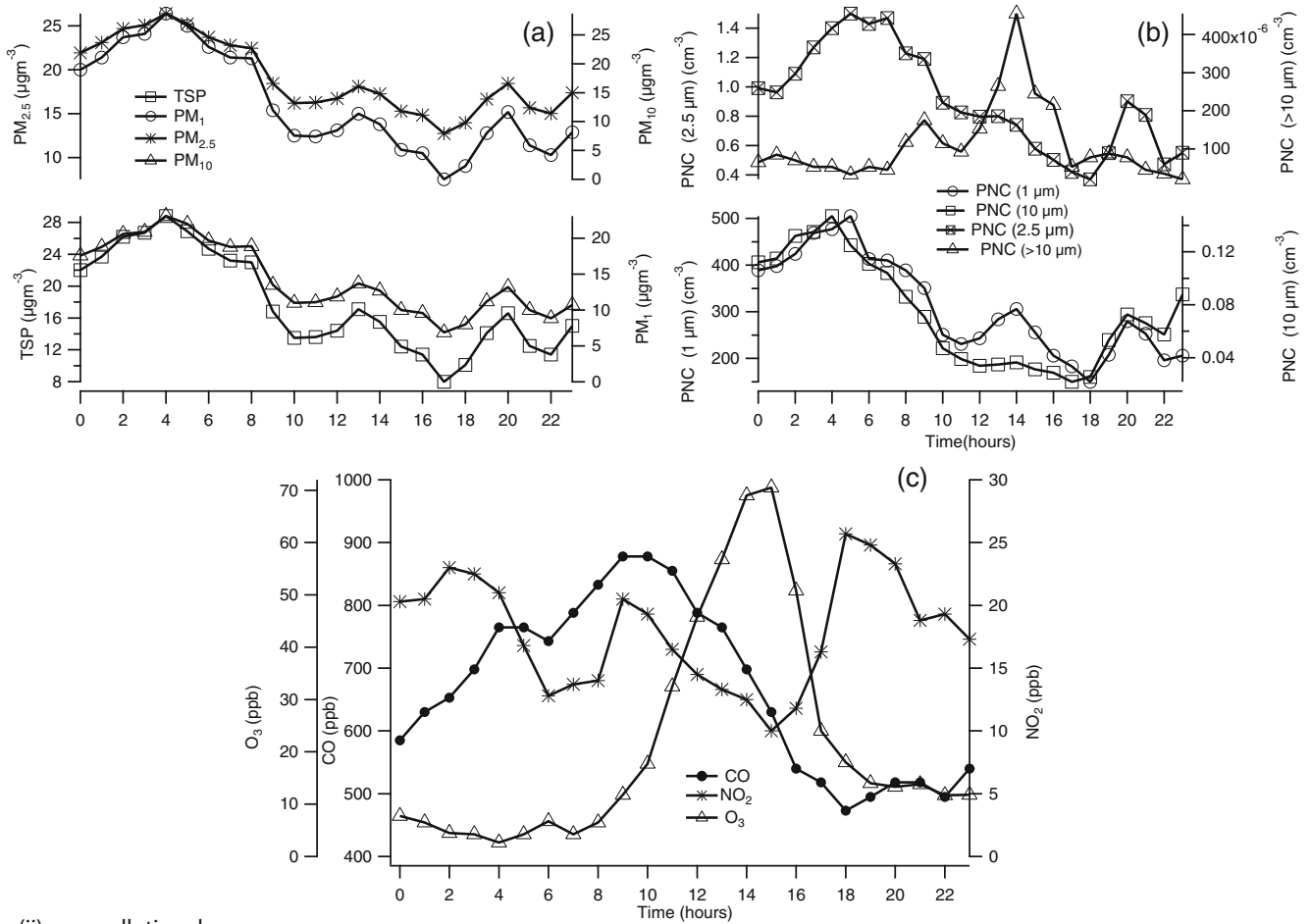
To determine the possible sources of PNC, PCA analysis followed by varimax rotation was conducted using the normalized dataset. The normalization of the variables was performed using the following equation to transform the dataset into a dimensionless standardized form

$$Z_{ik} = \frac{C_{ik} - \bar{C}_i}{\sigma_i} \quad (1)$$

where  $i = 1, 2, 3, \dots, n$ , the total number of elements in the data set,  $k = 1, 2, 3, \dots, m$ , the total number of observations,  $Z_{ik}$  is the standardized form of the value for variable  $i$ th and observation  $k$ ,  $C_{ik}$  is the concentration of  $i$ th variable and  $k$  observation,  $\bar{C}_i$  is the mean concentration of  $i$ th variable and all observations, and  $\sigma_i$  is the standard deviation of  $i$ th variable. Details of the procedure have been explained by Khan et al. (2010) and Thurston and Spengler (1985). PCA analysis identified five potential sources explaining 84.4 % of the total variance and an eigen value >1. Factor loadings of >0.70 for the variables were considered for interpretation. PC1 explained 43.8 % of the variance, and PNC was predominant in the fine and sub-micrometer range, 540 to 1800 nm. Thus, PC1 represents the particles in the fine and sub-micrometer mode. During the pollution episode, the smaller particles condense onto the surface of larger particles within an aged air mass which may contribute to the higher concentrations of larger particles noticed by Cusack et al. (2013). Therefore, the first factor score can be explained by fine and sub-micrometer mode aged particles. A 16.5 % of the variance has been explained by PC2 marking a significant factor loading for PNC in the range of 2250 to 7000 nm. Thus, PC2 addresses the coarse fraction of the PNC. A study by Silva et al. (1999) observed that the coarse mode ( $d > 1 \mu\text{m}$ ) particles are released from natural wildfires. Further, coarse particles in the aerodynamic size of ~3 μm are enriched with sea salt (Van Malderen et al. 1992). During the present study, natural wildfire or biomass burning originated mainly from regional or distant sources which are consistent with the origin of the trajectory as well as transport pathways of the air masses. PC3 included 12.4 % of the variance, and the significant factor loading shown by the variables, i.e. 9250 to 16,250 nm, represents coarser particles. The particles of sizes 4 to 15 μm are composed of aluminosilicates, one of the predominant compositions of windblown soil dust



(i) pollution days



(ii) non-pollution days

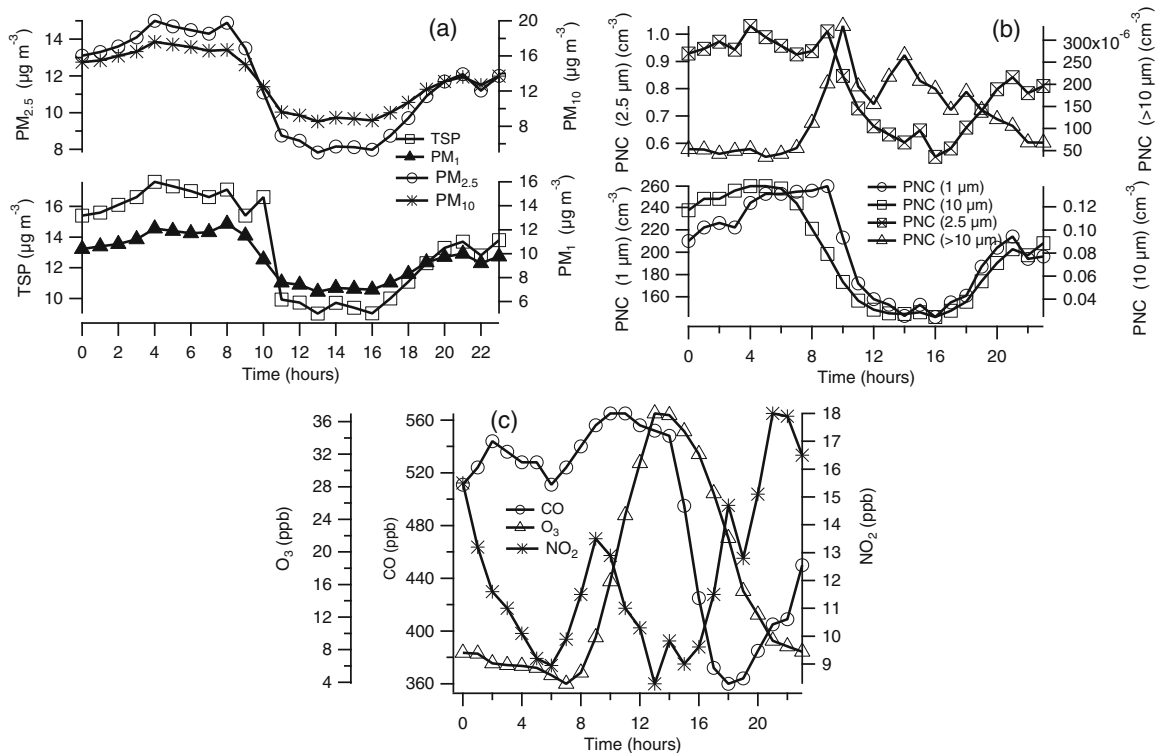


**Table 3** Spearman correlation coefficient (*r*) of particle mass and number concentration (PNC)

	TSP	PM <sub>10</sub>	PM <sub>2.5</sub>	PM <sub>1</sub>	N <sub>0.27</sub>	N <sub>0.29</sub>	N <sub>0.33</sub>	N <sub>0.38</sub>	N <sub>0.43</sub>	N <sub>0.48</sub>	N <sub>0.54</sub>	N <sub>0.62</sub>	N <sub>0.68</sub>	N <sub>0.75</sub>	N <sub>0.90</sub>	N <sub>1.15</sub>	N <sub>1.45</sub>	N <sub>1.80</sub>	N <sub>2.25</sub>	N <sub>2.75</sub>	N <sub>3.25</sub>	N <sub>3.75</sub>	N <sub>4.50</sub>	N <sub>5.75</sub>	
TSP	1																								
PM <sub>10</sub>	<b>1.00</b>	1																							
PM <sub>2.5</sub>	<b>0.98</b>	<b>0.99</b>	1																						
PM <sub>1</sub>	<b>0.96</b>	<b>0.96</b>	<b>0.99</b>	1																					
N <sub>0.27</sub>	<b>0.90</b>	<b>0.90</b>	<b>0.93</b>	<b>0.96</b>	1																				
N <sub>0.29</sub>	<b>0.90</b>	<b>0.91</b>	<b>0.94</b>	<b>0.96</b>	<b>0.99</b>	1																			
N <sub>0.33</sub>	<b>0.90</b>	<b>0.91</b>	<b>0.94</b>	<b>0.96</b>	<b>0.98</b>	<b>0.99</b>	1																		
N <sub>0.38</sub>	<b>0.90</b>	<b>0.91</b>	<b>0.93</b>	<b>0.94</b>	<b>0.95</b>	<b>0.97</b>	<b>0.99</b>	1																	
N <sub>0.43</sub>	<b>0.90</b>	<b>0.91</b>	<b>0.93</b>	<b>0.93</b>	<b>0.92</b>	<b>0.94</b>	<b>0.96</b>	<b>0.98</b>	1																
N <sub>0.48</sub>	<b>0.88</b>	<b>0.89</b>	<b>0.90</b>	<b>0.89</b>	<b>0.86</b>	<b>0.87</b>	<b>0.89</b>	<b>0.92</b>	<b>0.98</b>	1															
N <sub>0.54</sub>	<b>0.84</b>	<b>0.85</b>	<b>0.86</b>	<b>0.84</b>	<b>0.81</b>	<b>0.81</b>	<b>0.82</b>	<b>0.85</b>	<b>0.93</b>	<b>0.98</b>	1														
N <sub>0.62</sub>	0.78	0.79	<b>0.80</b>	0.77	0.73	0.72	0.72	0.74	<b>0.84</b>	<b>0.92</b>	<b>0.97</b>	1													
N <sub>0.68</sub>	0.75	0.76	0.77	0.74	0.69	0.68	0.68	0.69	0.79	<b>0.88</b>	<b>0.94</b>	<b>0.99</b>	1												
N <sub>0.75</sub>	0.72	0.72	0.74	0.71	0.67	0.66	0.65	0.65	0.75	<b>0.84</b>	<b>0.91</b>	<b>0.98</b>	<b>0.99</b>	1											
N <sub>0.90</sub>	0.70	0.71	0.72	0.69	0.65	0.63	0.62	0.62	0.72	<b>0.81</b>	<b>0.89</b>	<b>0.96</b>	<b>0.98</b>	<b>1.00</b>	1										
N <sub>1.15</sub>	0.66	0.66	0.68	0.65	0.61	0.59	0.57	0.57	0.66	0.75	<b>0.83</b>	<b>0.92</b>	<b>0.95</b>	<b>0.98</b>	<b>0.99</b>	1									
N <sub>1.45</sub>	0.61	0.61	0.63	0.59	0.56	0.53	0.51	0.50	0.59	0.68	0.77	<b>0.87</b>	<b>0.91</b>	<b>0.94</b>	<b>0.96</b>	<b>0.99</b>	1								
N <sub>1.80</sub>	0.64	0.64	0.63	0.56	0.51	0.49	0.47	0.48	0.57	0.67	0.75	<b>0.84</b>	<b>0.87</b>	<b>0.89</b>	<b>0.91</b>	<b>0.92</b>	<b>0.94</b>	1							
N <sub>2.25</sub>	0.71	0.72	0.66	0.56	0.49	0.49	0.51	0.53	0.59	0.67	0.69	0.70	0.70	0.67	0.67	0.64	0.64	<b>0.81</b>	1						
N <sub>2.75</sub>	0.68	0.70	0.62	0.52	0.45	0.46	0.49	0.52	0.56	0.62	0.62	0.59	0.57	0.52	0.51	0.46	0.45	0.63	<b>0.94</b>	1					
N <sub>3.25</sub>	0.66	0.68	0.60	0.50	0.43	0.44	0.47	0.50	0.54	0.60	0.59	0.55	0.53	0.48	0.47	0.42	0.40	0.58	<b>0.91</b>	<b>0.96</b>	1				
N <sub>3.75</sub>	0.58	0.60	0.52	0.42	0.36	0.37	0.40	0.44	0.47	0.54	0.52	0.49	0.47	0.42	0.41	0.36	0.35	0.54	<b>0.86</b>	<b>0.92</b>	<b>0.88</b>	1			
N <sub>4.50</sub>	0.55	0.56	0.48	0.39	0.35	0.35	0.39	0.42	0.44	0.48	0.46	0.41	0.38	0.33	0.32	0.27	0.25	0.42	<b>0.79</b>	<b>0.86</b>	<b>0.86</b>	<b>0.84</b>	1		
N <sub>5.75</sub>	0.26	0.26	0.20	0.15	0.12	0.14	0.16	0.19	0.17	0.16	0.13	0.08	0.06	0.05	0.04	0.03	0.04	0.15	0.35	0.37	0.38	0.39	0.40	1	

Values in bold are significant correlation coefficients (*r*) (*p*<0.05)

**Table 4** Predicted principal component (PC) factors to the particle number concentration (PNC)

Variables	PC1	PC2	PC3	PC4	PC5
<i>N</i> <sub>265</sub>	0.40	0.15	0.11	<b>0.86</b>	0.01
<i>N</i> <sub>290</sub>	0.38	0.16	0.08	<b>0.88</b>	0.01
<i>N</i> <sub>325</sub>	0.37	0.20	0.03	<b>0.89</b>	0.01
<i>N</i> <sub>375</sub>	0.40	0.23	−0.01	<b>0.87</b>	0.01
<i>N</i> <sub>425</sub>	0.55	0.20	−0.02	<b>0.79</b>	0.01
<i>N</i> <sub>475</sub>	0.67	0.22	−0.05	0.66	0.01
<i>N</i> <sub>540</sub>	<b>0.77</b>	0.18	−0.04	0.56	0.02
<i>N</i> <sub>615</sub>	<b>0.87</b>	0.14	−0.02	0.43	0.02
<i>N</i> <sub>675</sub>	<b>0.90</b>	0.12	−0.02	0.38	0.02
<i>N</i> <sub>750</sub>	<b>0.93</b>	0.10	0.01	0.34	0.02
<i>N</i> <sub>900</sub>	<b>0.94</b>	0.10	0.01	0.31	0.02
<i>N</i> <sub>1150</sub>	<b>0.95</b>	0.08	0.05	0.25	0.01
<i>N</i> <sub>1450</sub>	<b>0.95</b>	0.09	0.09	0.16	0.01
<i>N</i> <sub>1800</sub>	<b>0.89</b>	0.31	0.05	0.07	0.01
<i>N</i> <sub>2250</sub>	0.54	<b>0.79</b>	−0.08	0.12	0.04
<i>N</i> <sub>2750</sub>	0.26	<b>0.92</b>	−0.12	0.16	0.04
<i>N</i> <sub>3250</sub>	0.19	<b>0.94</b>	−0.14	0.15	0.04
<i>N</i> <sub>3750</sub>	0.16	<b>0.96</b>	−0.11	0.14	0.04
<i>N</i> <sub>4500</sub>	0.10	<b>0.98</b>	−0.04	0.13	0.03
<i>N</i> <sub>5750</sub>	0.02	<b>0.96</b>	0.06	0.14	0.01
<i>N</i> <sub>7000</sub>	0.02	<b>0.88</b>	0.27	0.14	−0.01
<i>N</i> <sub>8000</sub>	0.04	0.64	0.50	0.12	−0.14
<i>N</i> <sub>9250</sub>	0.10	0.31	<b>0.72</b>	0.06	−0.15
<i>N</i> <sub>11250</sub>	0.06	−0.01	<b>0.80</b>	0.07	−0.11
<i>N</i> <sub>13750</sub>	0.01	−0.13	<b>0.76</b>	0.00	−0.03
<i>N</i> <sub>16250</sub>	0.00	−0.18	<b>0.68</b>	0.04	−0.06
<i>N</i> <sub>18750</sub>	−0.04	−0.13	0.66	−0.01	0.00
<i>N</i> <sub>22500</sub>	0.02	−0.17	0.65	0.01	−0.21
<i>N</i> <sub>27500</sub>	−0.04	−0.06	0.16	−0.01	<b>−0.97</b>
<i>N</i> <sub>31000</sub>	0.01	−0.12	0.33	−0.03	0.02
<i>N</i> <sub>34000</sub>	−0.02	−0.02	0.04	−0.02	<b>−0.98</b>
Expl. var	8.31	6.97	3.63	5.24	2.02
Prp. totl	0.27	0.22	0.12	0.17	0.07
Eigen value	13.57	5.12	3.85	1.86	1.76
Total variance (%)	43.79	16.52	12.42	5.99	5.69
Cumulative (%)	43.79	60.31	72.73	78.72	84.40

Values in bold are stronger factor loadings that >0.70

(Kim et al. 2006; Van Malderen et al. 1992). Therefore, it is likely that particles in this size range mainly consist of soil dust that has been resuspended and transported from trans-boundary sources. PC4 has been explained by 6.0 % of the total variance and represents particles in the accumulation mode in the range of 265 to 425 nm. A study by Pey et al. (2009) described the PC dominating the accumulation mode

(575–800, 310–415, 415–575 nm) as released from an urban background source. A study conducted at an urban site by Harrison et al. (2011) observed a PC factor with a particle number distribution at 0.1 μm and the volume distribution of around 0.35 μm. Therefore, the accumulation mode particles in this factor score might originate from urban background sources. With respect to this station, the urban background site consists of the tropical rainforest, agriculture as well as road traffic or line sources. PC5 has shown 5.6 % of the total variance and is classified as giant particles, wind-blown from distance sources, in the aerodynamic size range of 27,500 to 34,000 nm. Similar observations were noted by Nicolás et al. (2009), where three factor components were identified as the accumulation mode (<0.9 μm), coarse (≥7.5 μm) and coarser particles i.e. wind resuspension of soil particles, respectively. Thus, the sources of PNC clearly demonstrate that the accumulation and sub-micrometer aged particles are predominantly released from local or background sources. In contrast, the coarse, coarser and giant particles might be abundant at this study location due to biomass burning, sea salt and windblown soil dust transported from distant sources.

**The lognormal distribution model**

The size distribution of aerosol can be determined as a function of particle diameter using the following lognormal equation (Birmili et al. 2001; Heintzenberg 1994):

$$y = A \exp \left[ \frac{(\ln d_{nm}(x) - \ln CMD)^2}{2(\ln \sigma)^2} \right] \tag{2}$$

where particle numbers and mass concentrations (*y*) were plotted against the logarithmic scale of the diameter (nm). The lognormal multiple fitting tool was employed using IGOR Pro, a graphical software (Wavemetrics, Lake Oswego, OR, USA) for the plots of number and mass concentrations to extract microphysical parameters such as the count median diameter (CMD), mass median diameter (MMD) and geometric standard deviation ( $\sigma_{gsd}$ ) of each mode. The size distribution of aerosol number concentration was determined for the month of February 2013 (Fig. 7), and this clearly shows a sharp uni-modal distribution in the accumulation mode (230.5 nm). Thus, the CMD for the accumulation mode in February 2013 was 230.5 nm. As shown in Tables 5 and 6, the geometric standard deviation ( $\sigma_{gsd}$ ) of number distribution in February 2013 was estimated as 1.2. The weekly CMDs were estimated as 233.9, 233.2, 233.6 and 228.4 nm for week 1 (WK1)-February 2013, week 2 (WK2)-February 2013, week 3 (WK3)-February 2013 and week 4 (WK4)-February 2013, respectively. The  $\sigma_{gsd}$  values were calculated as 1.2, 1.2, 1.2 and 1.3 for WK1-February 2013, WK2-February 2013, WK3-February 2013 and WK4-February 2013, respectively.

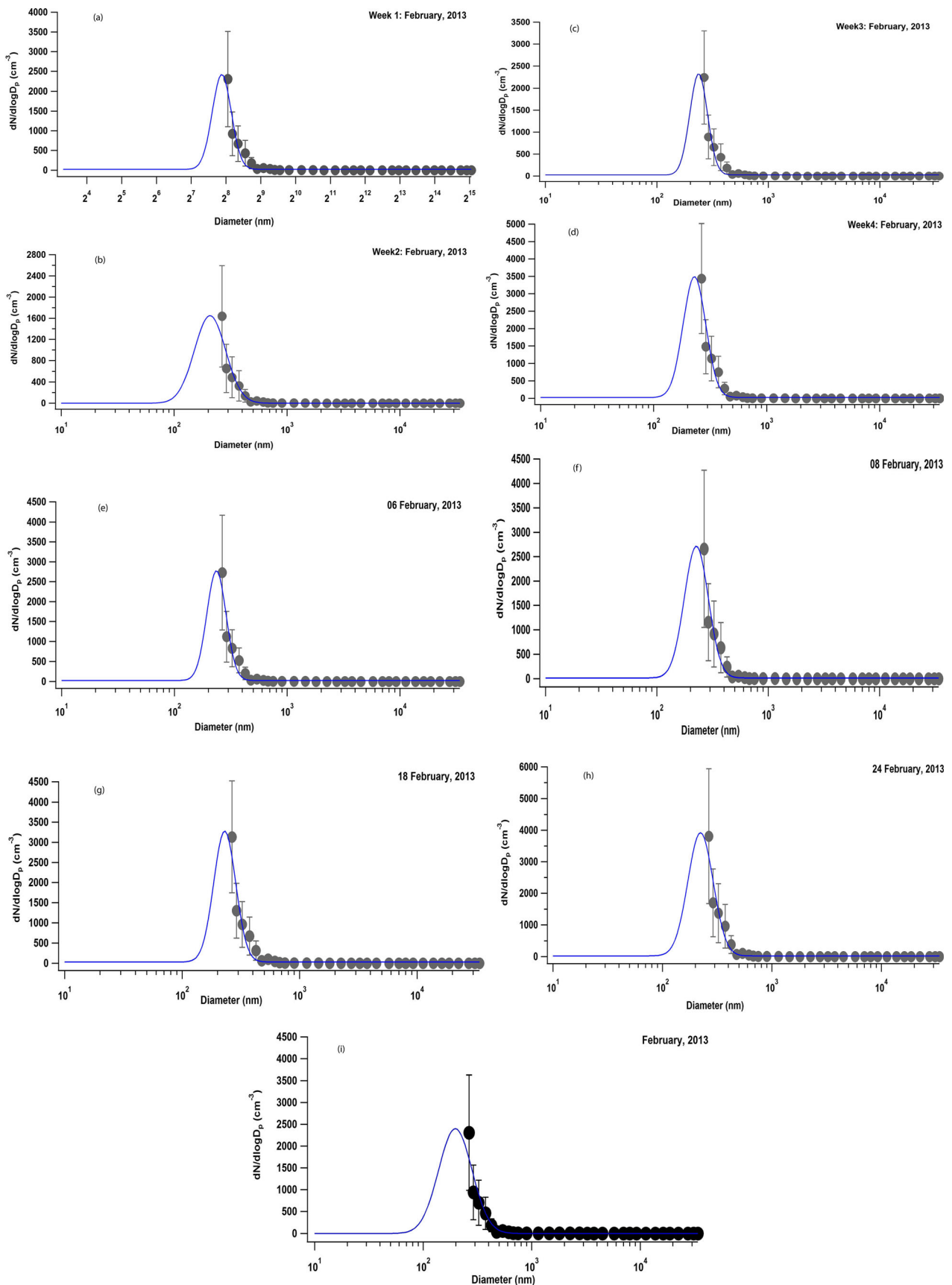


**Fig. 7** Size distribution of aerosol particle number concentration (PNC)

**Table 5** Estimated aerosol count median diameter (CMD), peak width and geometric standard deviation (GSD)

	CMD (nm)	Width (nm)	GSD
Overall February 2013	230.5	0.3	1.2
WK1-February 2013	233.9	0.3	1.2
WK2-February 2013	233.2	0.3	1.2
WK3-February 2013	233.6	0.3	1.2
WK4-February 2013	228.4	0.3	1.3
6/2/2013	233.7	0.3	1.2
8/2/2013	224.9	0.4	1.3
18/2/2013	195.0	0.5	1.4
24/2/2013	222.0	0.4	1.3

Likewise, the CMD was estimated for some polluted days in which we found high concentrations of particle numbers, and the resulting CMDs were 233.7, 224.9, 195.0 and 222.0 nm for 6, 8, 18 and 24 February 2013, respectively. The  $\sigma_{gsd}$  values for the selected daily sets of data were calculated as 1.2, 1.3, 1.4 and 1.3 for 6, 8, 18 and 24 February 2013, respectively. The geometric standard deviations for the weekly, daily and whole month number distributions in the accumulation mode varied from 1.6 to 1.8; these were nearly constant. A study conducted at the surface and above the Malaysian rainforest canopy reported that smaller fungal spores dominated particles in the range of 2–5  $\mu\text{m}$  (Gabey et al. 2010). Thus, the biological aerosol generated near the rainforest had an insignificant effect on the distribution of number concentration in the Bangi area. Furthermore, the diameter of the number size distribution shifted from 60 for clean to 80 nm for polluted days at the Peking University site in Beijing, China (Yue et al. 2009). The lognormal fitting model for the mass distribution of aerosol particles was subjected to the estimation of MMD and  $\sigma_{gsd}$  (Fig. 8). Unlike the number distribution, the results of this lognormal fitting

revealed that the two peaks were sharply and widely separated to produce a bimodal distribution. These results are consistent with the bimodal peaks of mass size distribution described in the previous work (Salam et al. 2012). The MMD of these two peaks were 189.2 and 2360.1 nm, with  $\sigma_{gsd}$  values of 1.7 and 1.8, respectively. The results suggested that the mass concentration was mainly associated with the fine and coarse mode, which is consistent with other studies in which a bimodal distribution was found in urban aerosol (Lonati et al. 2011; Tsai et al. 2011). Furthermore, by means of the lognormal fitting model (Table 6), the MMDs for the weekly data were estimated as 180.8, 198.0, 196.8 and 194.3 nm for WK1-February 2013, WK2-February 2013, WK3-February 2013 and WK4-February 2013, respectively, as presented in peak 1 (Fig. 8). The geometric standard deviations ( $\sigma_{gsd}$ ) of peak 1 were calculated as 1.8, 1.7, 1.7 and 1.7 for WK1-February 2013, WK2-February 2013, WK3-February 2013 and WK4-February 2013, respectively. The geometric standard deviation of MMD at peak 1 varied insignificantly, and the range of MMD was found to be 0.18–0.20  $\mu\text{m}$ . However, the particles of tropical biomass burning were confined to the fine mode at 0.33  $\mu\text{m}$  (Weinzierl et al. 2011), which was close to the MMD of peak 1. Likewise, the lognormal fit model was applied to the peak 2 into the weekly and selected daily data sets. As shown in Table 6, the MMD for the weekly data were observed as 2100.3, 2537.7, 2315.6 and 2400.0 nm for WK1-February 2013, WK2-February 2013, WK3-February 2013 and WK4-February 2013, respectively, as presented in peak 2 (Fig. 8). The geometric standard deviations ( $\sigma_{gsd}$ ) of peak 2 were estimated as 1.7, 1.7, 1.7 and 1.8 for WK1-February 2013, WK2-February 2013, WK3-February 2013 and WK4-February 2013, respectively. The results showed that the geometric standard deviations at this mode were also fairly stable. The results for MMD showed a range of 2.1–2.5  $\mu\text{m}$ , which represents dust particle aging and a shift from

**Table 6** and estimated aerosol mass median diameter (MMD), peak width and geometric standard deviation (GSD)

	Peak-1			Peak-2		
	MMD (nm)	Width (nm)	GSD	MMD (nm)	Width (nm)	GSD
Overall February 2013	189.2	0.8	1.7	2360.1	0.8	1.8
WK1-February 2013	180.8	0.8	1.8	2100.3	0.7	1.7
WK2-February 2013	198.0	0.7	1.7	2537.7	0.7	1.7
WK3-February 2013	196.8	0.7	1.7	2315.6	0.8	1.7
WK4-February 2013	194.3	0.8	1.7	2400.0	0.8	1.8
6/2/2013	205.0	0.7	1.6	2328.1	0.8	1.7
8/2/2013	195.9	0.7	1.7	2735.4	0.7	1.6
18/2/2013	180.0	0.9	1.9	1888.0	0.7	1.7
24/2/2013	190.5	0.8	1.8	1969.4	0.8	1.7

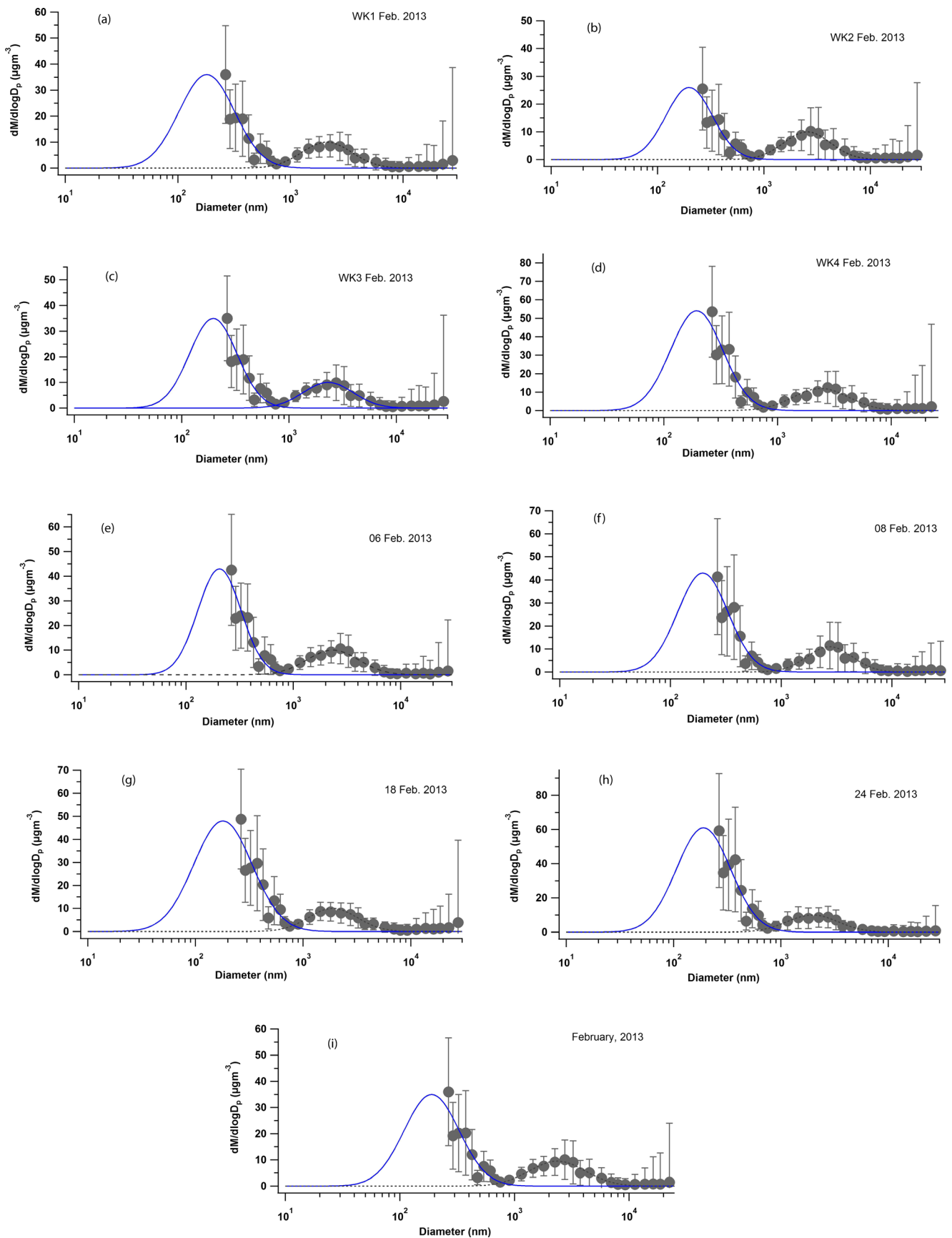


**Fig. 8** Size distribution of aerosol mass concentration

accumulation mode particles (Weinzierl et al. 2011). Likewise, sulphate and organic aerosol mass diameter exhibited a range of 170–270 nm in a clean atmosphere which was reported to be released from natural sources (Rimselyte 2007); this supports the results for peak 1 identified in this study.

### Conclusions

This study investigated the concentrations of particle mass and number concentration in a tropical semi-urban area. The variability of size-fractionated particle (TSP, PM<sub>10</sub>, PM<sub>2.5</sub> and PM<sub>1</sub>) concentrations in terms of local and synoptic meteorology, regional biomass fire hotspots, back trajectory analysis, correlation and PCA was determined. The mean concentrations of TSP, PM<sub>10</sub>, PM<sub>2.5</sub> and PM<sub>1</sub> were 14.37±4.43, 14.11±4.39, 12.53±4.13 and 10.53±3.98 µg m<sup>-3</sup> respectively, which are within the limits of the MAQG, WHO and US EPA guidelines. Particles in the accumulation mode (<500 nm) dominated the overall number concentration (99 %). This indicates that gas-to-particle conversion, adsorption on pre-existing particles and the growth of ultrafine particles due to the coagulation process have occurred. One per cent of particles were found to be in the coarse mode (>500 nm). Correlation analysis showed a strong correlation between PM<sub>1</sub> and PNC (*r*=0.99). Five potential factors resulted from the PCA analysis, and PC1 (43.8 % variance) predominated in terms of particle numbers in the fine and sub-micrometre range. PC2, PC3, PC4 and PC5 have explained 16.5, 12.4, 6.0 and 5.7 % of the variance to address the coarse, coarser, accumulation and giant fraction of PNC, respectively. The pronounced regional contribution to the concentration of particles, particularly on polluted days, was due to the northeasterly wind flow towards the Malaysian Peninsula. The PNC at the current location was substantially higher when compared to other locations in the world due to the complex aerosol system in this region. It also highlights the importance of further integrated aerosol studies, particularly into ultrafine particles. Our results were in good agreement with the MODIS distribution indication. We strongly recommend that the continued monitoring of high resolution PNC data covering the ultrafine range is undertaken. We also recommend that research on size distribution and new particle formation is carried out, in order to aid a more comprehensive understanding of the aerosol system in this study area.

**Acknowledgments** The authors would like to thank the Universiti Kebangsaan Malaysia for the Research University Grant (DIP-2012-020). We also would like to thank the Ministry of Education for the Fundamental Research Grant (FRGS/1/2013/STWN01/UKM/02/2). Special thanks to Ms K Alexander and Dr. Rose Norman for proofreading this manuscript.

### References

- Badarinath KVS, Madhavi Latha K, Kiran Chand TR, Gupta PK, Ghosh AB, Jain SL, Gera BS, Singh R, Sarkar AK, Singh N, Parmar RS, Koul S, Kohli R, Nath S, Ojha VK, Singh G (2004) Characterization of aerosols from biomass burning—a case study from Mizoram (Northeast), India. *Chemosphere* 54:167–175
- Birmili W, Wiedensohler A, Heintzenberg J, Lehmann K (2001) Atmospheric particle number size distribution in central Europe: statistical relations to air masses and meteorology. *J Geophys Res* 106:32005–32018
- Choi H, Choi DS (2008) Concentrations of PM<sub>10</sub>, PM<sub>2.5</sub>, and PM<sub>1</sub> influenced by atmospheric circulation and atmospheric boundary layer in the Korean mountainous coast during a duststorm. *Atmos Res* 89: 330–337
- Chow JC, Watson JG, Lowenthal DH, Hackney R, Magliano K, Lehman D, Smith T (1999) Temporal variations of PM<sub>2.5</sub>, PM<sub>10</sub> and gaseous precursors during the 1995 integrated monitoring study in central California. *J Air Waste Manage Assoc* 49:16–24
- Cusack M, Pérez N, Pey J, Alastuey A, Querol X (2013) Source apportionment of fine PM and sub-micron particle number concentrations at a regional background site in the western Mediterranean: a 2.5 year study. *Atmos Chem Phys* 13:5173–5187
- Cyrys J, Pitz M, Heinrich J, Wichmann HE, Peters A (2008) Spatial and temporal variation of particle number concentration in Augsburg, Germany. *Sci Total Environ* 401:168–175
- Draxler RR, Rolph GD (2013) HYSPLIT (HYbrid Single-Particle Lagrangian Integrated Trajectory) Model access via NOAA ARL READY Website (<http://ready.arl.noaa.gov/HYSPLIT.php>). NOAA Air Resources Laboratory, Silver Spring, MD
- Durant JL, Ash CA, Wood EC, Herndon SC, Jayne JT, Knighton WB, Canagaratna MR, Trull JB, Brugge D, Zamore W, Kolb CE (2010) Short-term variation in near-highway air pollutant gradients on a winter morning. *Atmos Chem Phys* 10:5599–5626
- Feng N, Christopher SA (2013) Satellite and surface-based remote sensing of Southeast Asian aerosols and their radiative effects. *Atmos Res* 122:544–554
- Gabey AM, Gallagher MW, Whitehead J, Dorsey JR, Kaye PH, Stanley WR (2010) Measurements and comparison of primary biological aerosol above and below a tropical forest canopy using a dual channel fluorescence spectrometer. *Atmos Chem Phys* 10:4453–4466
- Galindo N, Gil-Moltó J, Varea M, Chofre C, Yubero E (2013) Seasonal and interannual trends in PM levels and associated inorganic ions in southeastern Spain. *Microchem J* 110:81–88
- Grimm H, Eatough DJ (2009) Aerosol measurement: the use of optical light scattering for the determination of particulate size distribution, and particulate mass, including the semi-volatile fraction. *J Air Waste Manage Assoc* 59:101–107
- Harrison RM, Beddows DCS, Dall’Osto M (2011) PMF analysis of wide-range particle size spectra collected on a major highway. *Environ Sci Technol* 45:5522–5528
- Harshvardhan (1993) Chapter 3 aerosol-climate interactions. V.H. Peter (Ed.) International Geophysics, Academic Press
- Haywood J, Boucher O (2000) Estimates of the direct and indirect radiative forcing due to tropospheric aerosols: a review. *Rev Geophys* 38:513–543
- Heintzenberg J (1994) Properties of the log-normal particle size distribution. *Aerosol Sci Tech* 21:46–48
- Hinds WC (1999) Aerosol technology, properties, behavior, and measurement of airborne particles, 2nd edn. John Wiley & Sons, Inc., New York
- Hu X, Zhang Y, Ding Z, Wang T, Lian H, Sun Y, Wu J (2012) Bioaccessibility and health risk of arsenic and heavy metals (Cd, Co, Cr, Cu, Ni, Pb, Zn and Mn) in TSP and PM<sub>2.5</sub> in Nanjing, China. *Atmos Environ* 57:146–152

- Jacobson MZ (2002) Control of fossil-fuel particulate black carbon and organic matter, possibly the most effective method of slowing global warming. *J Geophys Res* 107(D19):4410
- Johansson C, Norman M, Gidhagen L (2007) Spatial & temporal variations of PM<sub>10</sub> and particle number concentrations in urban air. *Environ Monit Assess* 127:477–487
- Jung J, Kim YJ, Lee KY, Cayetano MG, Batmunkh T, Koo JH, Kim J (2010) Spectral optical properties of long-range transport Asian dust and pollution aerosols over Northeast Asia in 2007 and 2008. *Atmos Chem Phys* 10:5391–5408
- Kampa M, Castanas E (2008) Human health effects of air pollution. *Environ Pollut* 151:362–367
- Khan MF, Hirano K, Masunaga S (2010) Quantifying the sources of hazardous elements of suspended particulate matter aerosol collected in Yokohama, Japan. *Atmos Environ* 44:2646–2657
- Kim H, Hwang H, Ro C-U (2006) Single-particle characterization of soil samples collected at various arid areas of China, using low-Z particle electron probe X-ray microanalysis. *Spectrochim Acta B* 61:393–399
- Kittelson DB, Watts WF, Johnson JP (2004) Nanoparticle emissions on Minnesota highways. *Atmos Environ* 38:9–19
- Kittelson DB, Watts WF, Johnson JP (2006) On-road and laboratory evaluation of combustion aerosols—part I: summary of diesel engine results. *J Aerosol Sci* 37:913–930
- Leitte AM, Schlink U, Herbarth O, Wiedensohler A, Pan X-C, Hu M, Wehner B, Breitner S, Peters A, Wichmann HE, Franck U (2011) Associations between size-segregated particle number concentrations and respiratory mortality in Beijing, China. *Int J Environ Health Res* 22:119–133
- Lonati G, Ozgen S, Ripamonti G, Cernuschi S, Giugliano M (2011) Pedestrian exposure to size-resolved particles in Milan. *J Air Waste Manage Assoc* 61:1273–1280
- Meng X, Ma Y, Chen R, Zhou Z, Chen B, Kan H (2013) Size-fractionated particle number concentrations and daily mortality in a Chinese city. *Environ Health Perspect* 121:1174–1178
- Morales Betancourt R, Nenes A (2014) Understanding the contributions of aerosol properties and parameterization discrepancies to droplet number variability in a global climate model. *Atmos Chem Phys* 14:4809–4826
- Nicolás JF, Yubero E, Pastor C, Crespo J, Carratalá A (2009) Influence of meteorological variability upon aerosol mass size distribution. *Atmos Res* 94:330–337
- Pey J, Querol X, Alastuey A, Rodríguez S, Putaud JP, Van Dingenen R (2009) Source apportionment of urban fine and ultra-fine particle number concentration in a Western Mediterranean city. *Atmos Environ* 43:4407–4415
- Pope CA, Burnett RT, Thurston GD, Thun MJ, Calle EE, Krewski D, Godleski JJ (2004) Cardiovascular mortality and long-term exposure to particulate air pollution: epidemiological evidence of general pathophysiological pathways of disease. *Circulation* 109:71–77
- Pope CA, Dockery DW (2006) Health effects of fine particulate air pollution: lines that connect. *J Air Waste Manage Assoc* 56:709–742
- Ramanathan V, Crutzen PJ, Kiehl JT, Rosenfeld D (2001) Aerosols, climate, and the hydrological cycle. *Science* 294:2119–2124
- Reid JS, Hyer EJ, Johnson RS, Holben BN, Yokelson RJ, Zhang J, Campbell JR, Christopher SA, Di Girolamo L, Giglio L, Holz RE, Kearney C, Miettinen J, Reid EA, Turk FJ, Wang J, Xian P, Zhao G, Balasubramanian R, Chew BN, Janjai S, Lagrosas N, Lestari P, Lin N-H, Mahmud M, Nguyen AX, Norris B, Oanh NTK, Oo M, Salinas SV, Welton EJ, Liew SC (2013) Observing and understanding the Southeast Asian aerosol system by remote sensing: an initial review and analysis for the Seven Southeast Asian Studies (7SEAS) program. *Atmos Res* 122:403–468
- Richards LW (1983) Comments on the oxidation of NO<sub>2</sub> to nitrate—day and night. *Atmos Environ* 17:397–402
- Řimnáčová D, Ždímal V, Schwarz J, Smolík J, Řimnác M (2011) Atmospheric aerosols in suburb of Prague: the dynamics of particle size distributions. *Atmos Res* 101:539–552
- Rimselyte I (2007) Chemical composition and size distribution of fine aerosol particles on the east coast of the Baltic Sea. *Lith J Physic Tech Sci* 47:523–529
- Salam A, Mamoon HA, Ullah MB, Ullah SM (2012) Measurement of the atmospheric aerosol particle size distribution in a highly polluted mega-city in Southeast Asia (Dhaka-Bangladesh). *Atmos Environ* 59:338–343
- Seinfeld J, Pandis SN (2006) Atmospheric chemistry and physics: from air pollution to climate change. Wiley, New York
- Silva PJ, Liu D-Y, Noble CA, Prather KA (1999) Size and chemical characterization of individual particles resulting from biomass burning of local southern California species. *Environ Sci Technol* 33:3068–3076
- Technik GA (2006) GRIMM Ambient Dust Monitor # 365 USER MANUAL. Grimm Aerosol Technik GmbH, Ainring Germany
- Thurston GD, Spengler JD (1985) A quantitative assessment of source contributions to inhalable particulate matter pollution in metropolitan Boston. *Atmos Environ* 19:9–25
- Tsai J-H, Tzu-Chi Chang L, Huang Y-S, Chiang H-L (2011) Particulate composition characteristics under different ambient air quality conditions. *J Air Waste Manage Assoc* 61:796–805
- Van Malderen H, Rojas C, Van Grieken R (1992) Characterization of individual giant aerosol particles above the North Sea. *Environ Sci Technol* 26:750–756
- Wan Mahiyuddin WR, Sahani M, Aripin R, Latif MT, Thach T-Q, Wong C-M (2013) Short-term effects of daily air pollution on mortality. *Atmos Environ* 65:69–79
- Weber K, Vogel A, Fischer C, van Haren G, Pohl T (2010) Airborne measurements of the Eyjafjallajökull volcanic ash plume over north-western Germany with a light aircraft and an optical particle counter: first results. *Proc. SPIE* 7832, Lidar technologies, techniques, and measurements for atmospheric remote sensing VI, pp. 78320P-15
- Weinzierl B, Sauer D, Esselborn M, Petzold A, Veira A, Rose M, Mund S, Wirth M, Ansmann A, Tesche M, Gross S, Freudenthaler V (2011) Microphysical and optical properties of dust and tropical biomass burning aerosol layers in the Cape Verde region—an overview of the airborne in situ and lidar measurements during SAMUM-2. *Tellus Ser B Chem Phys Meteorol* 63:589–618
- Whitby KT, Clark WE, Marple VA, Sverdrup GM, Sem GJ, Willeke K, Liu BYH, Pui DYH (1975) Characterization of California aerosols—I. Size distributions of freeway aerosol. *Atmos Environ* 9:463–482
- Xian P, Reid JS, Atwood SA, Johnson RS, Hyer EJ, Westphal DL, Sessions W (2013) Smoke aerosol transport patterns over the Maritime Continent. *Atmos Res* 122:469–485
- Xiaoai G, Grimm H, Pesch M, Keck L, Spielvogel J, Schneider F, Brunnhuber W (2010) New methods for real-time measurement of environmental airborne particles, bioinformatics and biomedical engineering (ICBBE), 4th International Conference, pp. 1–4
- Xu J, Wang Z, Yu G, Sun W, Qin X, Ren J, Qin D (2013) Seasonal and diurnal variations in aerosol concentrations at a high-altitude site on the northern boundary of Qinghai-Xizang Plateau. *Atmos Res* 120–121:240–248
- Yue D, Hu M, Wu Z, Wang Z, Guo S, Wehner B, Nowak A, Achtert P, Wiedensohler A, Jung J, Kim YJ, Liu S (2009) Characteristics of aerosol size distributions and new particle formation in the summer in Beijing. *J Geophys Res* 114:D00G12
- Zhu Y, Hinds WC, Kim S, Sioutas C (2002) Concentration and size distribution of ultrafine particles near a major highway. *J Air Waste Manage Assoc* 52:1032–1042